LETTER

doi:10.1038/nature13586

Quantum imaging with undetected photons

Gabriela Barreto Lemos[1,2], Victoria Borish[1,3], Garrett D. Cole[2,3], Sven Ramelow[1,3]†, Radek Lapkiewicz[1,3] & Anton Zeilinger[1,2,3]

Information is central to quantum mechanics. In particular, quantum interference occurs only if there exists no information to distinguish between the superposed states. The mere possibility of obtaining information that could distinguish between overlapping states inhibits quantum interference[1,2]. Here we introduce and experimentally demonstrate a quantum imaging concept based on induced coherence without induced emission[3,4]. Our experiment uses two separate down-conversion nonlinear crystals (numbered NL1 and NL2), each illuminated by the same pump laser, creating one pair of photons (denoted idler and signal). If the photon pair is created in NL1, one photon (the idler) passes through the object to be imaged and is overlapped with the idler amplitude created in NL2, its source thus being undefined. Interference of the signal amplitudes coming from the two crystals then reveals the image of the object. The photons that pass through the imaged object (idler photons from NL1) are never detected, while we obtain images exclusively with the signal photons (from NL1 and NL2), which do not interact with the object. Our experiment is fundamentally different from previous quantum imaging techniques, such as interaction-free imaging[5] or ghost imaging[6–9], because now the photons used to illuminate the object do not have to be detected at all and no coincidence detection is necessary. This enables the probe wavelength to be chosen in a range for which suitable detectors are not available. To illustrate this, we show images of objects that are either opaque or invisible to the detected photons. Our experiment is a prototype in quantum information—knowledge can be extracted by, and about, a photon that is never detected.

The conceptual arrangement of our imaging technique, based on a quantum interference experiment[3,4] by Zou, Wang and Mandel, is illustrated in Fig. 1. A pump beam (green) divided by a 50:50 beam splitter (BS1) coherently illuminates two identical nonlinear crystals, NL1 and NL2, where pairs of collinear photons called signal (yellow) and idler (red) can be created ($|c\rangle|d\rangle$ in NL1 and $|e\rangle|f\rangle$ in NL2). The idler amplitude created in NL1 reflects at the dichroic mirror D1 into spatial mode d, and signal amplitude passes into spatial mode c. The idler passes through the object O of real transmittance coefficient T and phase shift γ: $|c\rangle_s|d\rangle_i \rightarrow Te^{i\gamma}|c\rangle_s|d\rangle_i + \sqrt{1-T^2}|c\rangle_s|w\rangle_i$, where for simplicity we lump all lost idler amplitude into a single state $|w\rangle_i$ (here subscripts s and i represent signal and idler). By reflection at dichroic mirror D2, the idler from NL1 aligns perfectly with idler amplitude produced at NL2, $|d\rangle_i \rightarrow |f\rangle_i$. The state at the grey dotted line is thus

$$\frac{1}{\sqrt{2}}\left[\left(Te^{i\gamma}|c\rangle_s + |e\rangle_s\right)|f\rangle_i + \sqrt{1-T^2}|c\rangle_s|w\rangle_i\right] \quad (1)$$

The idler is now reflected at the dichroic mirror D3 and discarded. The signal states $|c\rangle_s$ and $|e\rangle_s$ are combined at the 50:50 beam splitter BS2. The detection probabilities at the outputs $|g\rangle_s$ and $|h\rangle_s$, obtained by ignoring (tracing out) the idler modes, are

$$P_{g/h} = \frac{1}{2}[1 \pm T\cos\gamma] \quad (2)$$

Thus, fringes with visibility T can be seen at either output, even though the signals combined at BS2 have different sources[4,10]. These fringes appear in the signal single photon counts; the idlers are not detected. No coincidence detection is required.

The peculiar feature of this interferometer is that no detected photon has taken path d. Yet, in our experiment, it is precisely here where we put the object to be imaged. The key to this experiment is how the signal-source information carried by the undetected idler photon depends on T. For, if $T = 0$, an idler detected after D3, coincident with a signal count at $|g\rangle_s$ or $|h\rangle_s$, would imply the signal source was NL2. Detection of a signal photon without a coincident idler would imply the signal source was NL1. This which-source information destroys interference because it makes the quantum states overlapping at BS2 distinguishable. If $T = 1$, the idler photon carries no which-source information. The signal states overlapped at each output of BS2 are then indistinguishable; thus the interference term in equation (2) appears. The above arguments are valid even though the idler photons are not detected, for it is only the possibility of obtaining which-source information that matters in this experiment.

Our experiment has a connection to interaction-free measurements[11,12]. Note that $P_h = 0$ if no object is placed in the set-up ($T = 1$ and $\gamma = 0$). Now insert an opaque object ($T = 0$) so that $P_h > 0$, and monitor the idler reflection from D3. Coincident counts in $|h\rangle_s$ and the idler detector reveal that the object is present even though no photon interacted with the object. With our set-up it is thus possible to realize non-degenerate interaction-free imaging.

With O and D2 removed, equation (1) would be an ordinary two-particle entanglement[13], $|c\rangle_s|d\rangle_i + |e\rangle_s|f\rangle_i$. With them in, $|d\rangle_i \rightarrow Te^{i\gamma}|f\rangle_i$, which creates equation (1). A normal two-particle entanglement has changed into an interesting single-particle superposition, which is especially rich when T and γ are transverse-position dependent.

We expand the conceptual arrangement of Fig. 1 into an imaging system (Fig. 2). We replace the photon counters with cameras sensitive to single photons and the uniform object with one bearing features, that is, $T = T(x, y)$ and $\gamma = \gamma(x, y)$ depend on transverse position (x, y). Our source produces spatially entangled photon pairs[14,15]. Sharp spatial correlations between signal and idler in the object plane and confocal lens systems[16] (see Methods) guarantee a point-by-point correspondence between the object plane and the detector surface on the camera.

The intensity image (non-constant transmittance) is due to transverse-position-dependent which-source information carried by the undetected idler photons. The phase image is of a different nature: it is due to the fact that the position-dependent phase shift on the idler photons in path d is actually passed to the signal; that is[17], $|c\rangle_s\left(Te^{i\gamma}|f\rangle_i\right) + |e\rangle_s|f\rangle_i = \left(Te^{i\gamma}|c\rangle_s + |e\rangle_s\right)|f\rangle_i$. Remarkably, the idler beam $|f\rangle_i$ alone does not even carry the phase pattern, and without detection in coincidence it could not be used to obtain the phase image[18,19].

We will now show images obtained by detecting 810-nm photons with a camera capable of single-photon sensitivity at this wavelength, when three different objects are illuminated by 1,550-nm photons, to which our camera is blind (see Methods). First, a cardboard cut-out placed into the path D1–D2 is imaged. Next, we show that a position-dependent phase shift produces an image even when the object is opaque (an etched silicon plate) or invisible (etched silica plate) at the detection

[1]Institute for Quantum Optics and Quantum Information, Austrian Academy of Sciences, Boltzmanngasse 3, Vienna A-1090, Austria. [2]Vienna Center for Quantum Science and Technology (VCQ), Faculty of Physics, University of Vienna, A-1090 Vienna, Austria. [3]Quantum Optics, Quantum Nanophysics, Quantum Information, University of Vienna, Boltzmanngasse 5, Vienna A-1090, Austria. †Present address: Cornell University, 159 Clark Hall, 142 Science Drive, Ithaca, New York 14853, USA.

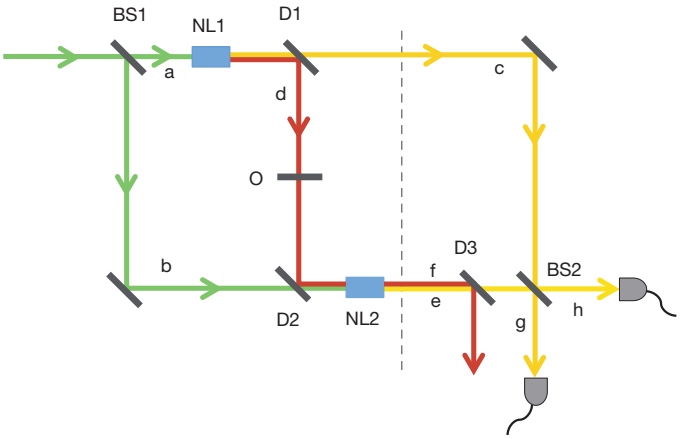

Figure 1 | Schematic of the experiment. Laser light (green) splits at beam splitter BS1 into modes a and b. Beam *a* pumps nonlinear crystal NL1, where collinear down-conversion may produce a pair of photons of different wavelengths called signal (yellow) and idler (red). After passing through the object O, the idler reflects at dichroic mirror D2 to align with the idler produced in NL2, such that the final emerging idler $|f\rangle_i$ does not contain any information about which crystal produced the photon pair. Therefore, signals $|c\rangle_s$ and $|e\rangle_s$ combined at beam splitter BS2 interfere. Consequently, signal beams $|g\rangle_s$ and $|h\rangle_s$ reveal idler transmission properties of object O.

wavelength. The images obtained with an electron multiplying charge coupled device (EMCCD) camera show single (non-heralded) counts per pixel (16 μm × 16 μm) obtained in an exposure time of 0.5 s with an electron multiplying gain factor of 20. The visibility achieved in the experiment is 77% (see Methods for details).

Figure 3a shows the beamsplitter output when a cardboard cut-out (illustrated in Fig. 3b) is inserted in the path D1–D2. Constructive interference is seen at one output of the beam splitter and destructive interference is observed in the other output. Interference only occurs in the region corresponding to the idler beam transmitted through the shape cut out of the cardboard, as seen in the sum and difference of the complementary images, shown in Fig. 3c and d, respectively. The sum of the two outputs of the beamsplitter gives the featureless intensity profile of the signal beams, demonstrating that the signal beams, while carrying the intensity information, are not absorbed at all by the mask.

In Fig. 4a, we show the image of an etched 500-μm-thick silicon plate; the plate is shown in Fig. 4b (see Methods section for details of the silicon plate and the etching process). Silicon is opaque to illumination at 810 nm,

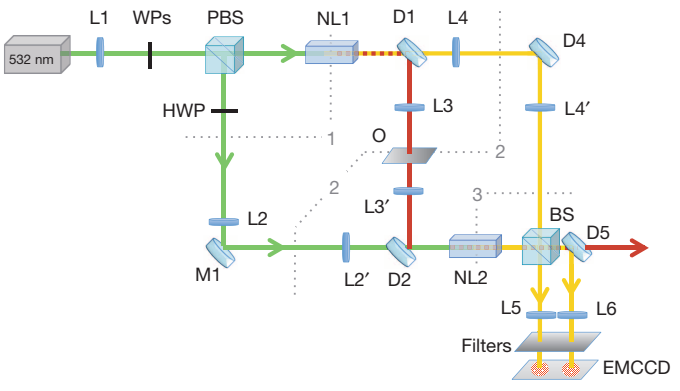

Figure 2 | Experimental set-up. A continuous-wave 532-nm laser (green) illuminates crystals NL1 and NL2. Wave plates (WPs) adjust the relative phase and intensity of the outputs of the polarizing beam splitter (PBS). The dichroic mirror D1 separates down-converted 810-nm (yellow) and 1,550-nm (red) photons. The 1,550-nm photons are transmitted through the object O and sent through NL2 by dichroic mirror D2. Lenses image plane 1 onto plane 3, and plane 2 onto the EMCCD camera. A 50:50 beam splitter (BS) combines the 810-nm beams. Dichroic mirrors D1, D2, D4 and D5 transmit the pump.

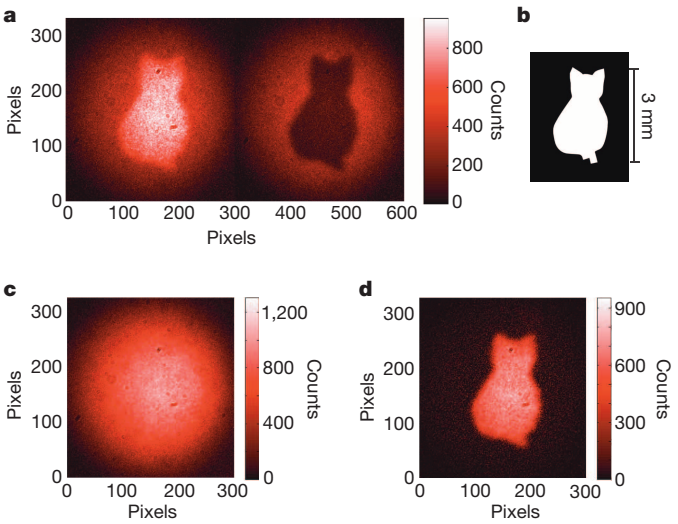

Figure 3 | Intensity imaging. **a**, Inside the cat, constructive and destructive interference are observed at the outputs of BS when we placed the cardboard cut-out shown in **b** in the path D1–D2. Outside the cat, idler photons from NL1 are blocked and therefore the signals do not interfere. **c**, The sum of the outputs gives the intensity profile of the signal beams. **d**, The subtraction of the outputs leads to an enhancement of the interference contrast, as it highlights the difference between constructive and destructive interference.

thus it is impossible to realize transmission imaging by illuminating the silicon with 810-nm photons. However, silicon is highly transparent at 1,550 nm and when we place the object in path D1–D2, the difference in optical path length for the etched and non-etched regions corresponds to a relative phase shift of π. Even though our camera is blind to 1,550-nm light, the image is seen by detecting 810-nm photons at the output of BS2 (Fig. 4a).

Finally, Fig. 5a shows the image of a fused silica (SiO_2) plate etched with a pattern that is invisible at the detection wavelength (details are given in the Methods section). We take advantage of the flexibility of our source to obtain collinear non-degenerate down-conversion at 820 nm

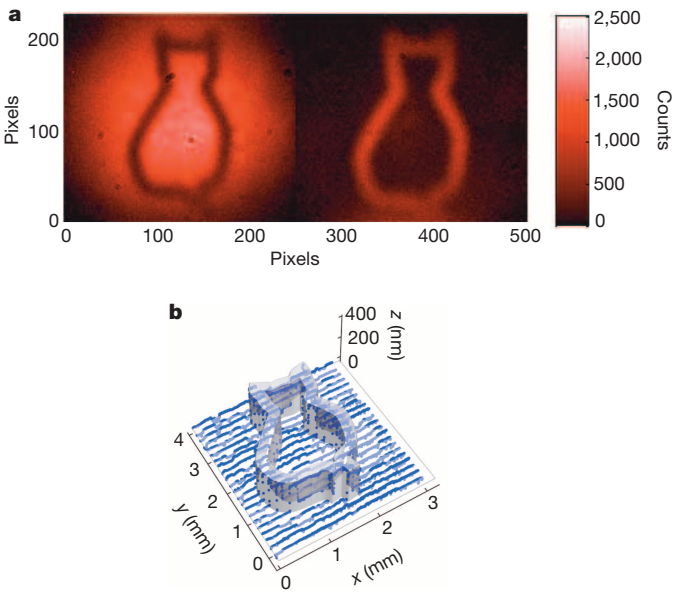

Figure 4 | Phase image of an object opaque to 810-nm light. **a**, Detection of 810-nm photons at both outputs of BS when a silicon plate (opaque to 810-nm light) with a 3-mm-tall etched cat (**b**) was introduced in path D1–D2. **b**, Three-dimensional rendering of the etch design overlaid with stylus profilometer scans (blue points) of the actual etch depth.

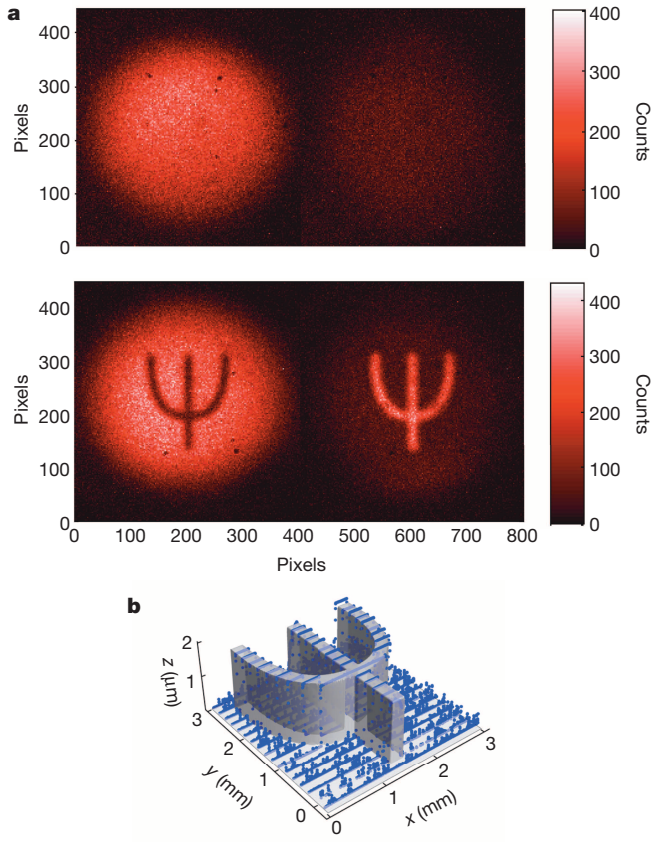

Figure 5 | Phase imaging of a 2π step at 820 nm. **a**, The top picture was taken with the object (shown in **b**) placed in the 820-nm beam between L4 and L4′; in the bottom picture, the object was placed in the 1,515-nm beam in path D1–D2. **b**, Three-dimensional rendering of the design overlaid with stylus profilometer scans (blue dots) of the actual etch depth.

and 1,515 nm (see Methods). The object (Fig. 5b) has an etch depth of 1,803 nm, imparting a relative phase shift of ~2π for 820-nm light. Thus the object is invisible when placed in the path of the detected photons between L4 and L4′ (top of Fig. 5a). This same etch depth gives an ~π phase step for 1,515-nm light, so when this same object is placed in the path D1–D2 of undetected photons, an image seen in the contrast of constructive to destructive interference is retrieved in the 820-nm outputs (bottom of Fig. 5a).

In summary, we have presented a quantum system for intensity and phase imaging where the photons that illuminate the object are not detected and the photons that are detected do not illuminate the object. We image objects that are either opaque or invisible at the detection wavelength (near-infrared) by illuminating three different objects with a wavelength to which our detector is blind. This experiment is fundamentally different to ghost imaging[6–9] as it relies on single-photon interference and does not require coincidence detection. Furthermore, our technique could be used for non-degenerate interaction-free imaging, with potential applications spanning biological imaging to the inspection of integrated circuits. Our system can realize grey-scale intensity or phase imaging, and it can be modified in order to measure spectral features (spectral imaging)[20].

We have demonstrated that our technique does not require the laser or the detector to function at the same wavelength as that of the light probing the object. Additionally, any nonlinear process can be used as a source, and this provides flexibility in the wavelength range for both detection and illumination of the object. In particular, in spontaneous parametric down-conversion (as used here), the only absolute restriction is that the sum of the two photon energies equals that of the pump photons. We have shown that information can be obtained about an object without detecting the photons that interacted with the object. Knowing the two-photon state, one can obtain information about an object. It has not escaped our attention that, on the other hand, by knowing the object, one could obtain information about the quantum state without detecting it.

METHODS SUMMARY

A detailed schematic of our imaging set-up is shown in Fig. 2. A 532-nm linearly polarized Gaussian pump laser beam focused by lens L1 on plane 1 is divided at a polarizing beam splitter (PBS) and coherently illuminates two identical periodically poled potassium titanyl phosphate (ppKTP) crystals, NL1 and NL2. The PBS plus wave plates (WPs) are used to control the relative amplitudes and phases between the reflected and transmitted pump beams. With an extra half-wave plate (HWP) in the reflected beam, both beams have the same polarization. The 1,550-nm idler amplitude produced at NL1 is reflected by dichroic mirror D1, through which the 810-nm signal and the pump are transmitted. Dichroic mirror D4 transmits 532-nm light and reflects 810-nm light. A long-pass filter (not shown in the figure) placed directly before the object O blocks any residual 532-nm or 810-nm light. The 1,550-nm amplitude from NL1 illuminates the object O and is then overlapped with the pump beam at dichroic mirror D2 that transmits 532-nm light and reflects 1,550-nm light.

Lens pairs L2–L2′, L3–L3′, and L4–L4′ image plane 1 onto plane 3, thereby ensuring that pump, idler and signal, respectively, are identical in these planes, thus contributing to obtain high interference visibility[21] (see Methods). Lenses L5 and L6 together with L3′ and L4′ image object plane 2 onto the camera surface.

The 810 ± 1.5 nm photons are detected (without heralding) in both outputs of the BS using an EMCCD camera that exhibits single-photon sensitivity at 810 nm, but has a negligible response at 1,550 nm.

Online Content Methods, along with any additional Extended Data display items and Source Data, are available in the online version of the paper; references unique to these sections appear only in the online paper.

Received 26 January; accepted 11 June 2014.

1. Feynman, R. P., Leighton, R. B. & Sands, M. *The Feynman Lectures on Physics* Vol. III, Chs 1 and 3 (Addison-Wesley, 1964).
2. Mandel, L. Coherence and indistinguishability. *Opt. Lett.* **16,** 1882–1883 (1991).
3. Zou, X. Y., Wang, L. J. & Mandel, L. Induced coherence and indistinguishability in optical interference. *Phys. Rev. Lett.* **67,** 318–321 (1991).
4. Wang, L. J., Zou, X. Y. & Mandel, L. Induced coherence without induced emission. *Phys. Rev. A* **44,** 4614–4622 (1991).
5. White, A. G., Mitchell, J. R., Nairz, O. & Kwiat, P. G. ''Interaction-free'' imaging. *Phys. Rev. A* **58,** 605–613 (1998).
6. Abouraddy, A. F., Stone, P. R., Sergienko, A. V., Saleh, B. E. A. & Teich, M. C. Entangled-photon imaging of a pure phase object. *Phys. Rev. Lett.* **93,** 213903 (2004).
7. Gatti, A., Brambilla, E. & Lugiato, L. Quantum imaging. *Prog. Opt.* **51,** 251–348 (2008).
8. Pittman, T. B. *et al.* Two-photon geometric optics. *Phys. Rev. A* **53,** 2804–2815 (1996).
9. Aspden, R. S., Tasca, D. S., Boyd, R. W. & Padgett, M. J. EPR-based ghost imaging using a single-photon-sensitive camera. *New J. Phys.* **15,** 073032 (2013).
10. Wiseman, H. M. & Mølmer, K. Induced coherence with and without induced emission. *Phys. Lett. A* **270,** 245–248 (2000).
11. Elitzur, A. C. & Vaidman, L. Quantum mechanical interaction-free measurements. *Found. Phys.* **23,** 987–997 (1993).
12. Kwiat, P., Weinfurter, H., Herzog, T., Zeilinger, A. & Kasevich, M. A. Interaction-free measurement. *Phys. Rev. Lett.* **74,** 4763–4766 (1995).
13. Horne, M. in *Experimental Metaphysics* Vol. 1. (eds Cohen, R. S., Horne, M. & Stachel, J.) 109–119 (Kluwer Academic, 1997).
14. Howell, J. C., Bennink, R. S., Bentley, S. J. & Boyd, R. W. Realization of the Einstein-Podolsky-Rosen paradox using momentum-and position-entangled photons from spontaneous parametric down conversion. *Phys. Rev. Lett.* **92,** 210403 (2004).
15. Walborn, S. P., Monken, C. H., Pádua, S. & Souto Ribeiro, P. H. Spatial correlations in parametric down-conversion. *Phys. Rep.* **495,** 87–139 (2010).
16. Tasca, D. S., Walborn, S. P., Souto Ribeiro, P. H., Toscano, F. & Pellat-Finet, P. Propagation of transverse intensity correlations of a two-photon state. *Phys. Rev. A* **79,** 033801 (2009).
17. Horne, M. A., Shimony, A. & Zeilinger, A. Two particle interferometry. *Phys. Rev. Lett.* **62,** 2209–2212 (1989); Two particle interferometry. *Nature* **347,** 429–430 (1990).
18. Ribeiro, P. H. S., Pádua, S., Machado da Silva, J. C. & Barbosa, G. A. Controlling the degree of visibility of Young's fringes with photon coincidence measurements. *Phys. Rev. A* **49,** 4176–4179 (1994).
19. Abouraddy, A. F., Stone, P. R., Sergienko, A. V., Saleh, B. E. A. & Teich, M. C. Entangled-photon imaging of a pure phase object. *Phys. Rev. Lett.* **93,** 213903 (2004).
20. Zou, X. Y., Grayson, T. P. & Mandel, L. Observation of quantum interference effects in the frequency domain. *Phys. Rev. Lett.* **69,** 3041–3044 (1992).

21. Grayson, T. P. & Barbosa, G. A. Spatial properties of spontaneous parametric down-conversion and their effect on induced coherence without induced emission. *Phys. Rev. A* **49,** 2948–2961 (1994).

Acknowledgements We thank M. Horne for reading the manuscript, clarifying suggestions and many discussions, P. Enigl for designing the figures for the objects, D. Greenberger and S. von Egan-Krieger for discussions, and C. Schaeff for equipment loans. Microfabrication was carried out at the Center for Micro- and Nanostructures (ZMNS) of the Vienna University of Technology. We acknowledge D. Ristanic for assistance with cryogenic Si etching and M. Schinnerl for contact mask production. G.B.L. was funded by the Austrian Academy of Sciences (ÖAW) through a fellowship from the Vienna Center for Science and Technology (VCQ). S.R. is funded by an EU Marie Curie Fellowship (PIOF-GA-2012-329851). This project was supported by ÖAW, the European Research Council (ERC Advanced grant no. 227844 'QIT4QAD', and SIQS grant no. 600645 EU-FP7-ICT), and the Austrian Science Fund (FWF) with SFB F40 (FOQUS) and W1210-2 (CoQus).

Author Contributions A.Z. initiated this research. G.B.L., V.B., R.L., S.R. and A.Z. designed the experiment. G.B.L., V.B. and R.L. carried out the experiment. G.D.C. fabricated the silicon and silica phase masks. All authors contributed to the writing of the manuscript.

Author Information Reprints and permissions information is available at www.nature.com/reprints. The authors declare no competing financial interests. Readers are welcome to comment on the online version of the paper. Correspondence and requests for materials should be addressed to G.B.L. (gabriela.barreto.lemos@univie.ac.at) and A.Z. (anton.zeilinger@univie.ac.at).

METHODS

Down-conversion sources. The 532-nm pump beam is generated by a frequency-doubled diode-pumped solid-state laser (Coherent Sapphire SF) and is focused onto the two periodically poled potassium titanyl phosphate (ppKTP) crystals with dimension 1 mm × 2 mm × 2 mm and poling period 9.675 μm for type-0 phase matching. The crystals are spatially oriented so down-conversion occurs when the CW pump beam is horizontally polarized (both the signal and idler produced are also horizontally polarized). In order to conform to the phase-matching conditions for 810-nm and 1,550-nm photons, NL1 (NL2) is heated to 83.7 °C (84.7 °C). When the set-up is adjusted to produce 820-nm and 1,515-nm photons (to be used with the fused silica phase object), NL1 (NL2) is heated to 39.2 °C (39.7 °C). All images were obtained with 150-mW pump power.

Wavelength filtering. Inside the interferometer, D1 is used to separate the 810-nm photons from the 1,550-nm photons. Mirror D1 (and also D2) reflects about 93% of 1,550-nm light and transmits about 99% of 810-nm light. Most of the pump beam going through NL1 is transmitted through both D1 and D4 (each with a transmittance of around 97% at 532 nm) and therefore almost never reaches BS. The dichroic mirror D5 additionally transmits some 532-nm light (around 25%), so some of the pump beam that goes through NL2 as well as some of the remaining pump beam from NL1 are discarded there. All remaining pump beam light is eliminated with either filters or the imaging object itself. The silicon sample is opaque to both 532-nm and 810-nm light, thus completely blocking these wavelengths along the path D1–D2. When the other samples are used, a long-pass filter is placed just before the object to cut out these lower wavelengths. The remaining 532-nm light that is not separated out through the dichroic mirrors or object is blocked in front of the camera by three filters. A 3-nm narrowband filter centred at 810 nm and two long pass filters were attached directly to the front of the camera. As it utilizes a silicon-based detector, the camera (Andor Luca-R EMCCD) does not detect 1,550-nm photons. Nonetheless, a combination of spectral filters guarantees that neither 1,550-nm photons nor 532-nm pump photons reach the camera.

Imaging lens systems. As it is crucial that the down-converted photons be identical, we use confocal lens systems to image plane 1 onto plane 3 (see Fig. 2), thus ensuring that the pump beams at NL1 and NL2 are identical, the 810-nm photons when they combine at the BS are identical, and the 1,550-nm photons are identical from NL2 onward. Lenses L2 and L2′ image plane 1 of the pump onto plane 3, and similarly L3 (L4) and L3′ (L4′) image plane 1 onto plane 3 for the 1,550-nm (810-nm) photons. Lenses L5 and L6 in combination with L4′ image plane 2 onto the EMCCD camera. Lenses L2, L2′, L3, L3′, L4, L4′ have a focal length of $F_1 = 75$ mm. The distance from plane 1 to each of L2, L3 and L4 is 75 mm; from those lenses to plane 2 is another 75 mm; from plane 2 to L2′, L3′ and L4′ is also 75 mm; and from those lenses to plane 3 is yet another 75 mm. This ensures that the photons produced in both crystals have the same waist and divergence when they reach the BS. Lenses L5 and L6 have a focal length of $F_2 = 150$ mm. They are placed 150 mm after plane 3 and 150 mm before the camera. The total imaging magnification from the object to the camera is given by $\frac{F_2\lambda_s}{F_1\lambda_i}$, where λ_s and λ_i are the wavelengths of the signal and idler photons, respectively.

Optical path lengths. In our single photon interferometer the paths D1–D4–BS and D1–D2–BS need to be equal, even though no detected photons actually follow the entire path D1–D2–BS. To assure indistinguishability of the emission in the two crystals (NL1 and NL2) the time delay between the arrival of the signal and idler for each of the two crystals must be the same. The path length difference between the signal and idler for the pair from NL1 is the distance NL1–D1–D2–BS subtracted from the distance NL1–D1–D4–BS. The path length difference between the signal and idler for the pair from NL2 is zero since the down-conversion is collinear. Thus, we see that the optical path lengths between D1–D4–BS and D1–D2–BS must be equal to within the coherence length of the photons. The coherence length of the photons is in our case determined by the filtering (3 nm), so we approximate the coherence length to be 0.2 mm. The other relevant optical path lengths are the paths PBS–D1–D2–NL2 and PBS–M1–NL2. The differential distance between these paths must be within the coherence length of the laser, which in our case is approximately 200 m.

Intensity object. Our intensity object is constructed from 0.33-mm-thick card stock with images defined by laser cutting. The images on the object were each 3 mm high.

Microfabricated silicon phase sample. The first custom phase sample consists of 500-μm-thick double-side polished (100)-oriented single-crystal silicon with imaging targets defined on one face using standard microfabrication techniques. The absorption coefficient of silicon is $\sim$1,000 cm^{-1} at 810 nm (ref. 22), and it is $\sim 10^{-4}$ cm^{-1} at 1,550 nm (ref. 23). Processing begins by cleaving a 75-mm-diameter silicon wafer to obtain chips with lateral dimensions of 25 mm × 25 mm. The cleaved chips are patterned using conventional optical contact lithography followed by plasma etching. In order to generate a relative π-phase shift at 1,550 nm, features are etched to a depth of approximately 310 nm (nominal height of 321 nm using a refractive index of silicon of 3.48; ref. 24) into the exposed Si surface using a cryogenic (−108 °C) SF_6/O_2 reactive-ion etching (RIE) process protected with a positive photoresist mask. To improve thermal transfer, the silicon chips are mounted on a carrier wafer using a thin layer of vacuum grease. Additionally, in order to minimize variations in the overall etch depth and thus resulting phase shift from the imaging targets, the feature linewidth is kept constant over the lithographic pattern to mitigate the effects of aspect-ratio dependent etching (or 'RIE lag'). After etching, the chips are removed from the carrier wafer and the masking resist and mounting film are stripped using a combination of organic solvents and oxygen plasma ashing. In order to eliminate spurious reflections from the polished surfaces, a dual-sided silicon nitride anti-reflection (AR) coating is deposited via plasma-enhanced chemical vapour deposition (PECVD) using He-diluted SiH_4 and NH_3 as reactive process gases. The deposition process yields quarter-wave optical thickness layers at a target film thickness of 2,040 Å (with a refractive index of 1.9 at the imaging wavelength of 1,550 nm).

In order to achieve the highest contrast, the relative path-length difference between the etched and non-etched regions should be equal to a half wavelength of 1,550-nm light adjusted for the difference in the indices of refraction of silicon and air. This gives a target thickness difference of 321 nm (for a refractive index of silicon of 3.48). Given the slight error in etch depth, the actual thickness difference is 310 nm, which is still sufficient to obtain high contrast images.

Microfabricated fused silica phase sample. Similar to the silicon phase object described above, the fused silica phase sample, cleaved from a 500-μm-thick glass wafer, is constructed via a standard lithographic and reactive ion etching process. In this case the same mask pattern is once again defined with contact lithography. In order to transfer the features into the fused silica, a high-power inductively coupled plasma (ICP) RIE process is required (150 W ICP, 250 W RF powers) with an etch chemistry consisting of SF_6 and Ar. Given the poor selectivity to the masking resist, a thick (10 μm) coating of AZP4620 photoresist is required. The target etch depth of 1,788 nm is achieved within roughly 10 min at room temperature. Given the high plasma energy, thermalization with the cooled carrier wafer is key. Due to non-uniformities in thermal contact with the carrier, we observe significant variation in etch depth (±200 nm) across the surface of the 25 mm × 25 mm pattern. No AR coating is employed given the small Fresnel reflection (4%) from the low-index silica substrate.

For 820-nm light, an exact 2π phase shift is given by a thickness difference of 1,811 nm (using an index of refraction of 1.45)[25]; after processing, the average etch depth recorded for the fused silica sample is 1,803 nm.

Interference visibility. In order to quantify the visibility in our imaging experiment, we detect the total intensity of 810-nm photons at one output of BS as a function of the relative phase between the pump beams that illuminate each crystal. Extended Data Fig. 1 shows a plot of the count rate measured with an avalanche photodiode when no object is present. The red circles show the experimental points, and the best fitting sinusoidal function (red line) gives a visibility of (77 ± 1)%. The visibility for our experiment is given not only by losses in both the 1,550-nm and 810-nm arms of the interferometer, but also by residual imperfections in the alignment for the two idler beams. The blue squares correspond to data obtained when the path NL1–NL2 is completely blocked, which results in zero interference visibility. Interference only arises if the idler between the two crystals is unblocked, for only then is its source, and therefore also the source of its signal sister, unknowable.

Showing that induced emission is negligible in the experiment. In order to demonstrate in our experiment that the 1,550-nm photons from NL1 do not induce down-conversion in NL2, we show in Extended Data Fig. 2 the count rates for 810-nm photons originating at NL2 when the 1,550-nm beam between D1 and D2 was blocked (blue crosses) and unblocked (red dots). The mean count rate and the standard deviation were obtained by analysing data obtained over 40 s. The blue diamonds show that the ratio of the count rates for the blocked and unblocked configuration is very close to 1 irrespective of the pump power.

22. Jellison, G. E. Jr. & Modine, F. A. Optical absorption of silicon between 1.6 and 4.7 eV at elevated temperatures. *Appl. Phys. Lett.* **41,** 180 (1982).
23. Khalaidovski, A., Steinlechner, J. & Schnabel, R. Indication for dominating surface absorption in crystalline silicon test masses at 1550 nm. *Class. Quantum Grav.* **30,** 165001 (2013).
24. Malitson, I. H. Interspecimen comparison of the refractive index of fused silica. *J. Opt. Soc. Am.* **55,** 1250 (1965).
25. Bass, M. *Handbook of Optics* Vol. 2, 2nd edn (Optical Society of America, 1995).

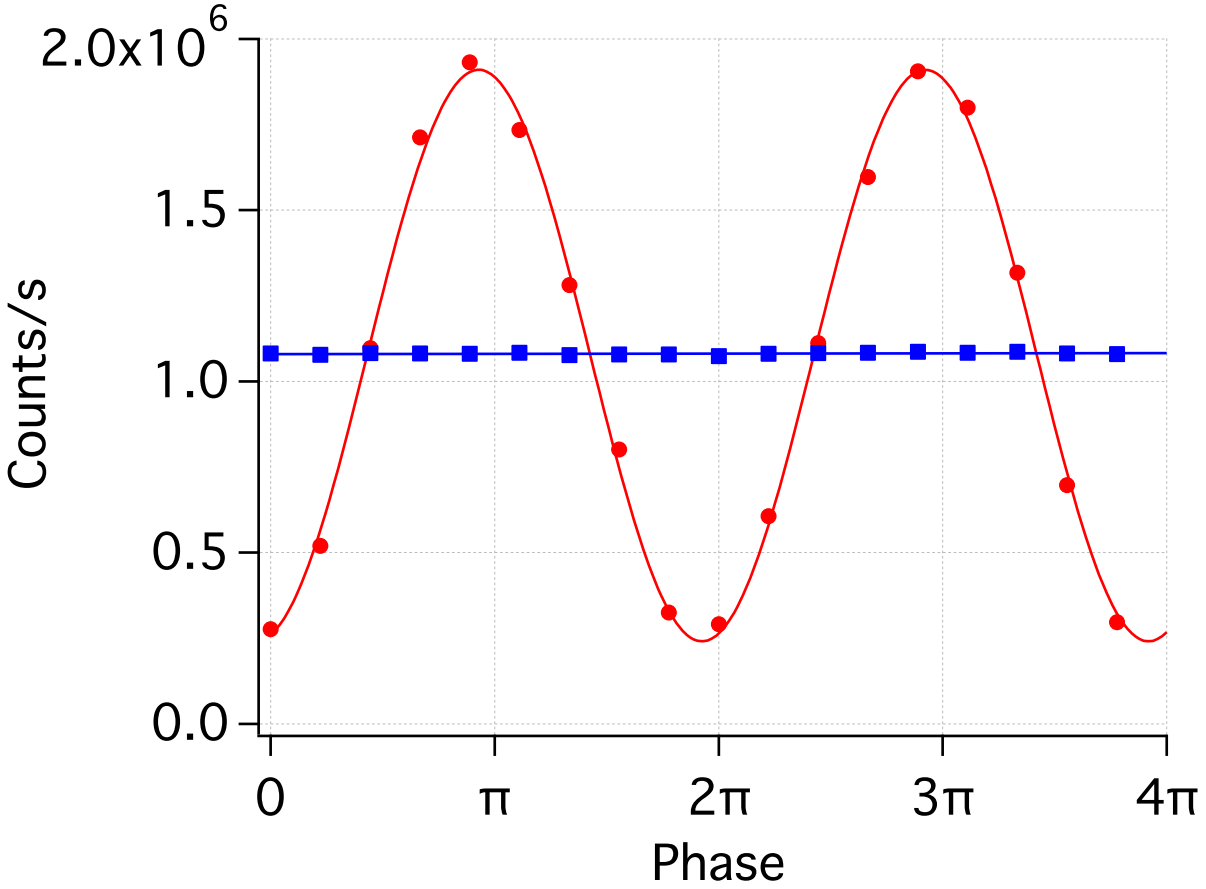

Extended Data Figure 1 | Visibility of the experiment. The count rates were recorded with the path D1–D2 both unblocked (red dots) and blocked (blue squares) as the relative phase between the transmitted and reflected beams of the PBS was varied. The red line is a sine curve fit for the experimental data giving (77 ± 1)% visibility. The error bars are smaller than the size of the data points.

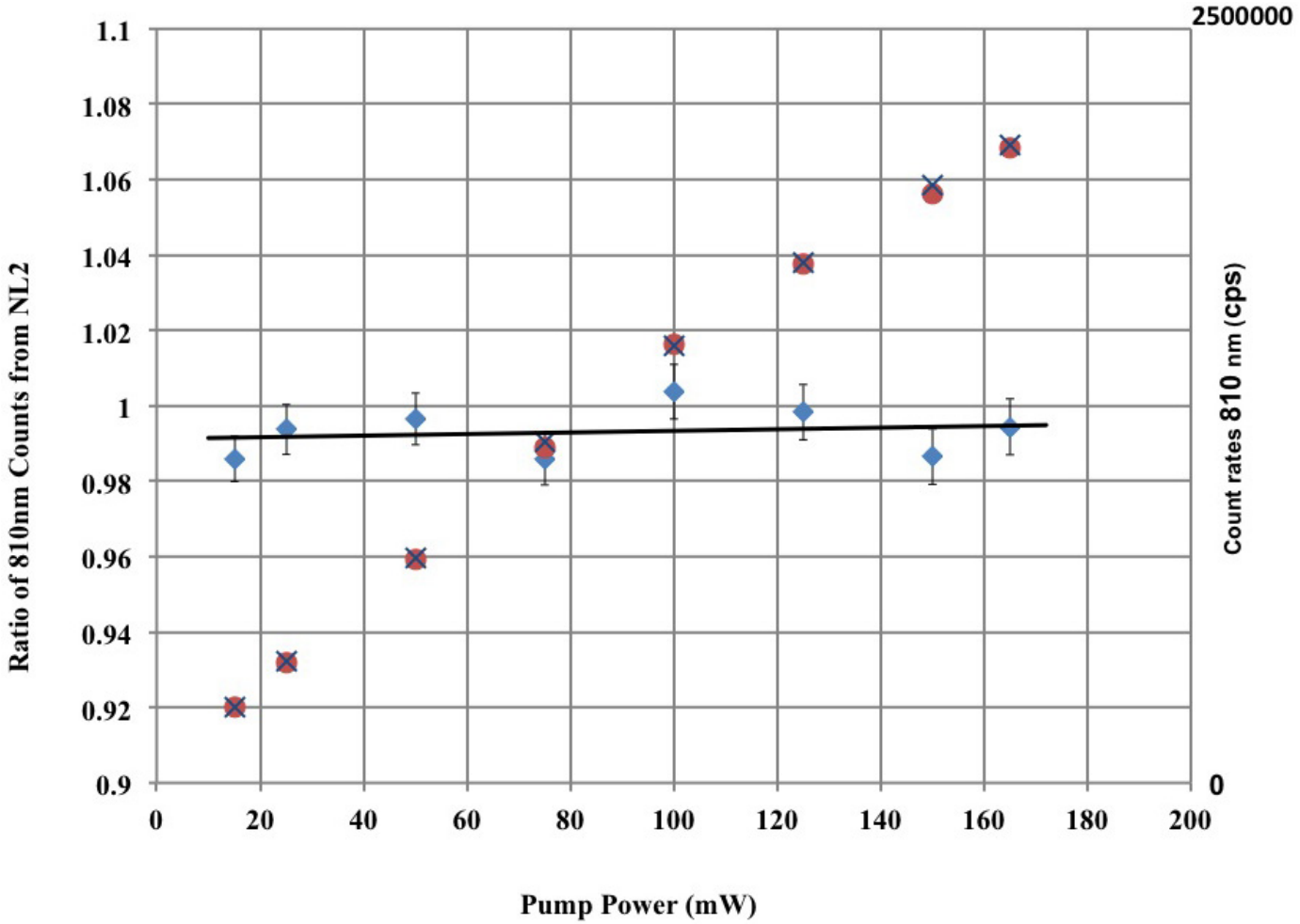

Extended Data Figure 2 | Excluding induced emission. Shown are the count rates for 810-nm photons produced in NL2 when the path between D1 and D2 was blocked (blue crosses) and unblocked (red dots). The blue diamonds show the ratio of the count rates for the blocked and unblocked configuration. The linear fit for this data (black line) gives an angular coefficient of $(2 \pm 4) \times 10^{-5}$ $(\mathrm{mW})^{-1}$.